IEEE Access
Multidisciplinary : Rapid Review : Open Access Journal

Received December 30, 2021, accepted February 8, 2022, date of publication February 11, 2022, date of current version February 22, 2022.

Digital Object Identifier 10.1109/ACCESS.2022.3151128

A New Multi-Output DC-DC Converter for Electric Vehicle Application

MUDADLA DHANANJAYA[1], DEVENDRA PONURU[2], (Senior Member, IEEE), THANIKANTI SUDHAKAR BABU[3], (Senior Member, IEEE), BELQASEM ALJAFARI[4], AND HASSAN HAES ALHELOU[5], (Senior Member, IEEE)

[1]Department of Electrical and Electronics Engineering, Anil Neerukonda Institute of Technology and Sciences, Visakhapatnam 531162, India
[2]Department of Electrical and Electronics Engineering, Gayatri Vidya Parishad College of Engineering for Women, Kommadi, Visakhapatnam 530048, India
[3]Department of Electrical and Electronics Engineering, Chaitanya Bharathi Institute of Technology, Hyderabad 500075, India
[4]Electrical Engineering Department, College of Engineering, Najran University, Najran 11001, Saudi Arabia
[5]Department of Electrical Power Engineering, Faculty of Mechanical and Electrical Engineering, Tishreen University, Lattakia, Syria

Corresponding author: Hassan Haes Alhelou (alhelou@ieee.org)

ABSTRACT Multiport converters play a significant role in portable electronic and electric vehicle (EV) applications. In literature, different configurations of single-input multi-output (SIMO) converters are presented. Most of the SIMO converters generate the outputs with operating constraints on the duty ratio and charging of inductors. The cross-regulation problem is still a challenge in SIMO converters design. A SIMO topology is proposed in this study to overcome the limitations mentioned earlier. It can generate three different output voltages without constraint on the duty cycle and inductor currents (like $i_{L1} > i_{L2} > i_{L3}$ or $i_{L1} < i_{L2} < i_{L3}$). Cross regulation problems do not exist in the proposed topology, so the load voltage V_{01} (V_{02}) (V_{03}) is not affected by the variation of output current i_{03} (i_{02}) (i_{01}). The loads are isolated from each other during control. In the laboratory, a 200 W prototype circuit is developed; simulation and experimental results are validated.

INDEX TERMS Multiport converters, single input multi output converters.

I. INTRODUCTION

In the past decade, there has been an increase in demand for renewable energy sources utilization in electric vehicles (EVs), auxiliary power, and grid-connected applications [1]–[5]. In these applications, multiport DC-DC converters are essential for Hybridizing energy sources which lead to, reduce the components count, complexity, and cost of the system compared to several separate single input DC-DC converters [6], [7].

Over the past decade, MPC converters have been presented. A new SIMO converter is proposed in [8]. This structure simultaneously generates boost, buck, and inverted outputs controlled independently. However, producing 'n' voltage levels requires n + 2 switches, which increases the overall size and cost of the converter. Unexpected mistakes in calculating state-space equations and output voltages for a SIMO converter given in [8] are addressed and rectified in [9]. The single coupled inductor-based SIMO buck is presented in [10] with lesser output inductor current ripple than single inductor SIMO converters. Nayak and Nath [11] elaborately presented the comparative performance of SIDO converters based on the coupled inductor and single inductor (SI) in terms of cross-coupling issues. Furthermore, they proposed that the coupled inductor SIDO converter has a better steady-state and transient performance. Nevertheless, in a SI SIMO configuration inductor is switched between the loads, which causes high ripples and cross-regulation problems.

Different control approaches are proposed in the literature to overcome the cross-regulation issue in a single inductor-based SIMO converter; the current predictor controller is presented in [12] instead of the conventional charge-balance approach. However, generating the duty ratios for active switches has been somewhat complicated. Similarly, the deadbeat-based control approach is presented in [13]. It is based on output current observer, and hence it is sensitive to the noise and significant parametric variations. In [14], a multivariable digital controller-based SIMO converter is proposed to minimize the voltage ripples, suppress the cross-regulation problems, and regulate the output voltages. However, controller design may lead to an increase in complexity.

The associate editor coordinating the review of this manuscript and approving it for publication was Zhilei Yao.

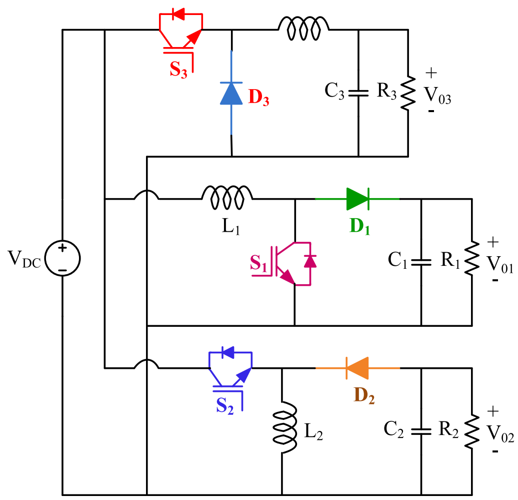

FIGURE 1. Diagram of conventional SIMO converter.

A non-isolated and single switch SIMO converter topology is presented in [15]. It has fewer components and reduces the cost of the system. However, it may be challenging to regulate the outputs independently.

To alleviate the problems in a single inductor SIMO converter, a non-isolated SIMO converter is proposed in [16]–[25], which are independently regulated the output voltages and does not require an additional control circuit. In [16], a new SIDO converter topology is proposed to integrate buck and super lift converter for generating the step-up and step-down output voltages for electrical vehicle applications. It has a constraint on-duty ratio viz. $D_2 < D_1$, which limits the operation range of D_1 by increasing D_2. The topologies proposed in [17] and [18] have fewer semiconductor switches. However, the operation of the converter is based on the charging time of inductors (i.e., $i_{L1} > i_{L2}$). So this keeps the constraint on-duty ratio.

The combination of high gain step-up and SEPIC converter-based SIMO is suggested for PV applications in [19]. In this configuration, both the outputs are higher than the supply voltage and improve the output voltage by adding the capacitors and diodes. Nevertheless, the number of capacitors and diodes affects cost and conduction losses. A new SIDO buck-boost topology is developed in [20] to generate positive and negative outputs. A multi-output converter is suggested in [21] with the reduced part count. However, it has more diodes, which increases conduction losses. A structure of SIMO configuration is introduced in [22] with the advantages of reducing the passive filter size and low voltage stress. High-density multi-output converter is proposed in [23] for portable electronic applications based on the front-end switched-capacitor technique with improved power density and reduced switching losses.

Modified SEPIC and interleaved-based high step-up SIMO converter are introduced in [24]. It consists of a voltage multiplier, coupled inductor, and switched capacitors to boost the output voltage in sustainable energy applications. However, it has complexity due to more components. The SEPIC-Cuk converter-based four-phase interleaved converter is suggested for SIMO applications in [25]. It has the advantages of low ripple voltage, compact size and is suitable for high power applications with a dynamic response.

In the conventional approach, EVs' auxiliary power supply system to handle the load requirements is shown in Figure 1. It looks simple, but the main drawback of this approach is a cross-regulation problem, and the loads are not isolated from each other during their operation. There is also the chance of grounding issues while charging the battery with simultaneously turn-on loads and if the ground is involved. Further, the circuit complexity will increase to convert one of the negative output voltages into buck-boost operation mode.

In the proposed work, the onboard power converter is the main subject of the study. The configuration of the circuit shown in Figure 2(a) is such that energy stored in the inductor is confined to one output only and is not shared with the other outputs during the control, which allows regulating the output voltages with independent duty-cycles. More importantly, the loads are isolated from each other during control, and the cross-regulation problem is successfully eliminated. Also, there are no problems associated with grounding as it is an onboard power converter even if charging of battery and ground is involved.

The remaining sections of the article are organized as follows: The developed SIMO configuration and modes of operation are presented in Section II. Small-signal modeling is presented in Section III. The controller design, parameter design, power loss analysis, and comparative assessment are discussed in Section IV. The simulation and experiment and results are shown in Section V. Summarized in Section VI.

II. PROPOSED SIMO CONFIGURATION AND MODES OF OPERATION

The proposed single input three-output DC-DC configuration is depicted in Figure 2(a). In this configuration the components are as follows, input voltage V_{DC}, switches (S_1-S_3), diodes (D_1-D_3), and passive elements (L_1-C_1, L_2-C_2, and L_3-C_3). It can generate three different output voltages, i.e., boost (V_{01}), buck-boost (V_{02}) with positive voltage polarity, and buck (V_{03}). The proposed converter is suitable for independently regulating the output voltages by the duty cycles D_1, D_2, *and* D_3, respectively. The theoretical waveforms of circuit elements are depicted in Figure 2(b).

The proposed configuration is different from the conventional parallel combination of buck, boost, and buck-boost configuration. In the proposed circuit configuration, the loads are isolated during the simultaneous control. From the following figures, one may observe that during mode-1operation, load R_3 alone through S_3 is connected to the input power supply, but the other loads are isolated, as shown in Figure 3(a). Similarly, during mode-2 only load R1 alone through D_1 is connected to the input supply, but other loads are isolated, as depicted in Figure 3(b). In the proposed control strategy, all the loads are isolated from each other during their control in any mode of operation. However, this feature is impossible

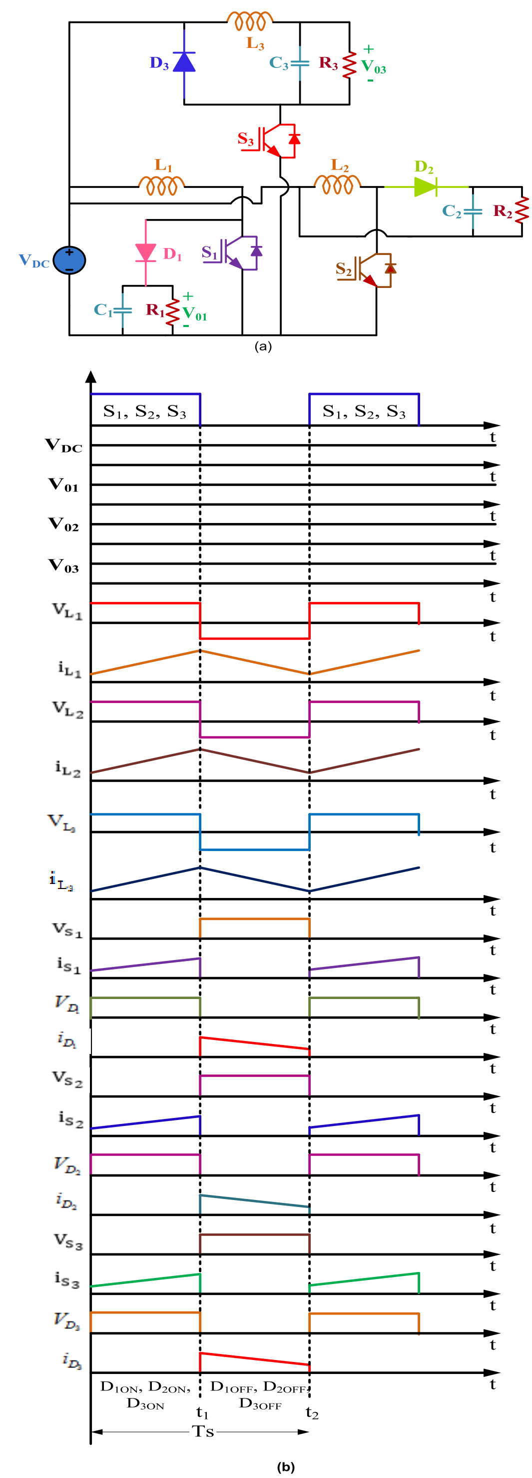

FIGURE 2. Proposed configuration: (a) SIMO configuration, (b) Theoretical waveforms.

in the conventional parallel combination of buck, boost, and buck-boost converters.

This circuit configuration looks very simple, but it is novel and valuable. A comparison in terms of the number of components, modes of operation, and working conditions between the conventional and proposed SIMO converter is presented in Table 1, as given below

TABLE 1. Parameter specification comparison between the conventional and proposed SIMO converter.

Comparison different aspects	Conventional	Proposed
Number of components	6	6
Output voltage	Buck, Boost, and Buck-Boost **(Negative output voltage)**	Buck, Boost, and Buck-Boost **(Positive output voltage)**
Inverting circuit is required for the positive output voltage	Yes	No
Loads are isolated to each other during control	No	Yes

In the conventional approach shown in Figure1, the main drawback is the cross-regulation problem, and the loads are not isolated from each other during their operation. Further, the circuit complexity will increase to convert the negative polarity of output voltages in the buck-boost mode of operation.

The proposed structure has the following advantages:

a) It is a simple structure and no assumptions on operating duty ratio ($D_1 > D_2 > D_3$ or $D_3 < D_2 < D_1$ or $D_1 = D_2 = D_3$)
b) It can generate three different output voltages, i.e., boost, buck, buck-boost()
c) No constraints on inductor currents (like $i_{L1} > i_{L2} > i_{L3}$ or $i_{L1} < i_{L2} < i_{L3}$ or $i_{L1} = i_{L2} = i_{L3}$)
d) Loads are isolated from each other during control and the cross-regulation problem is successfully eliminated
e) It gives the positive buck-boost output voltage

A. MODES OF OPERATION

1) SWITCHING STATE 1

Switches S_1, S_2, and S_3 are turned ON. The current flow path is depicted in Figure 3(a), and the energy port V_{DC} magnetizes L1, L2, and L3. Consequently, the C_1 and C_2 are discharged to the loads (R_1) and (R_2), respectively, whereas (C_3) is charged. The inductor currents and capacitor voltages are represented in Eq. (1)-(4).

$$i_{L_1}(t) = \frac{V_{DC}}{L_1}t + i_{L1(0)}, \quad v_{C_1}(t) = v_{C1(0)}e^{\frac{-1}{R_1C_1}t} \tag{1}$$

$$i_{L_2}(t) = \frac{V_{DC}}{L_2}t + i_{L2(0)}, \quad v_{C_2}(t) = v_{C2(0)}e^{\frac{-1}{R_2C_2}t} \tag{2}$$

$$i_{L_3}(t) = \frac{V_{DC}}{R_3} + e^{-\alpha t}\left[c_1 \cos\omega_d t + c_2 \sin\omega_d t\right] \tag{3}$$

$$v_{C_3}(t) = V_{DC} - \frac{L_3}{2C_3}e^{-\alpha t}\begin{bmatrix} \cos\omega_d t(\frac{\alpha c_1}{R_3} + \omega_d c_2) \\ +\sin\omega_d t(-\alpha c_2 + \frac{\omega_d c_1}{R_3}) \end{bmatrix} \tag{4}$$

2) SWITCHING STATE 2

In this state, L_1, L_2, and L_3 are de-magnetized and deliver their energy to the load through D_1, D_2, and D_3, respectively.

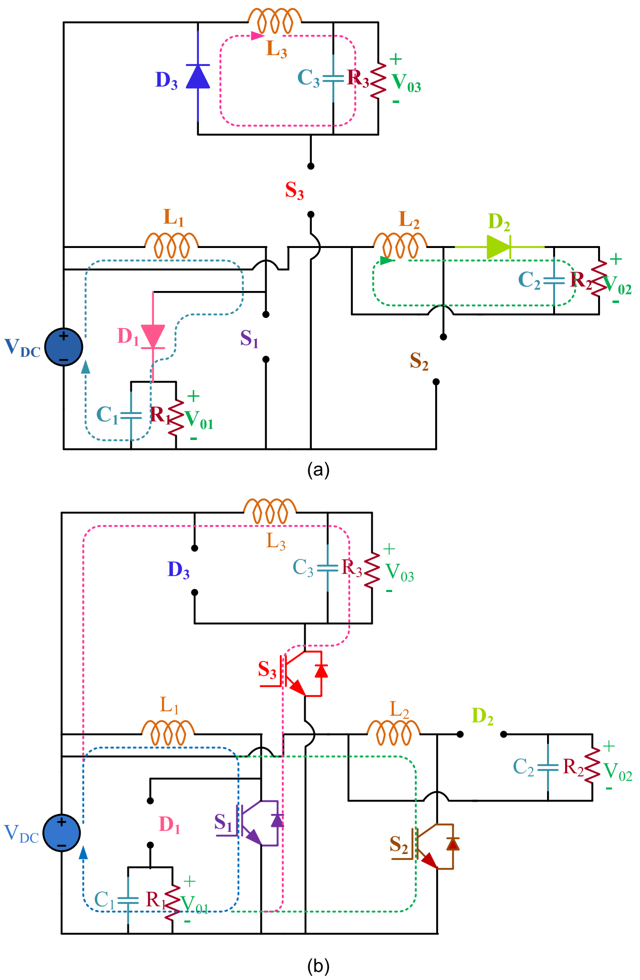

FIGURE 3. Operating states: (a) Switching state-1 and (b) Switching state-2.

It is illustrated in Figure 3(b). The inductor currents and capacitor voltages are in Eq. (5)–(11) as follows,

$$i_{L_1}(t) = \frac{V_{DC}}{R_1} + e^{-\alpha_1 t}\left[c_1 \cos\omega_{d1}t + c_2 \sin\omega_{d1}t\right] \tag{5}$$

$$v_{C_1}(t) = V_{DC} - \frac{L_1}{2C_1}e^{-\alpha_1 t}\left[\begin{array}{l}\cos\omega_{d1}t(\frac{c_1}{R_1} - \omega_{d1}c_2) \\ +\sin\omega_{d1}t(\omega_{d1}c_1 + \frac{c_2}{R_1})\end{array}\right] \tag{6}$$

$$i_{L_2}(t) = e^{-\alpha_2 t}\left[c_3 \cos\omega_{d2}t + c_4 \sin\omega_{d2}t\right] \tag{7}$$

$$v_{C_2}(t) = -L_2 e^{-\alpha_2 t}\left[\begin{array}{l}(-\alpha_2 c_3 + \omega_{d2}c_4)\cos\omega_{d2}t \\ +(\omega_{d2}c_3 - \alpha_2 c_4)\sin\omega_{d2}t\end{array}\right] \tag{8}$$

$$i_{L_3}(t) = e^{-\alpha t}\left[c_5 \cos\omega_d t + c_6 \sin\omega_d t\right] \tag{9}$$

$$v_{C_3}(t) = -L_3 e^{-\alpha t}\left[\begin{array}{l}(-\alpha c_5 + \omega_d c_6)\cos\omega_d t \\ +(\omega_d c_5 - \alpha c_6)\sin\omega_d t\end{array}\right] \tag{10}$$

$$\alpha_1 = \frac{1}{2R_1C_1}, \quad \omega_{d1} = \frac{1}{2}\sqrt{\left(\frac{1}{R_1^2C_1^2} - \frac{4}{L_1C_1}\right)},$$

$$\alpha_2 = \frac{1}{2R_2C_2} \quad \text{and}\ \omega_{d2} = \frac{1}{2}\sqrt{\left(\frac{1}{R_2^2C_2^2} - \frac{4}{L_2C_2}\right)}$$

$$\alpha = \frac{1}{2R_3C_3}, \quad \omega_d = \frac{1}{2}\sqrt{\left(\frac{1}{R_3^2C_3^2} - \frac{4}{L_3C_3}\right)}, \tag{11}$$

where c_1, c_2, c_3, c_4, c_5, and c_6 areinitial values.

Output voltages of the proposed configuration are as follows

$$V_{01} = \frac{V_{DC}}{(1-D_1)}, \quad V_{02} = \frac{V_{DC}D_2}{(1-D_2)}, \ V_{03} = D_3V_{DC} \tag{12}$$

D_1, D_2, and D_3 are duty ratios of the S_1, S_2, and S_3 respectively.

It is observed that during switching state-1operation, load (R_3) alone through S_4 is connected to the ground but the other loads are isolated even when the ground is involved during charging the battery, as shown in Figure 3(a). Similarly, during switching state-2 only load (R_1) alone through D_1 is connected to the ground, but other loads are isolated from the ground and the load (R_1) as well as depicted in Figure 3(b). In the proposed control strategy, all the loads are isolated from each other during their control during any mode of operation. Moreover, the configuration of the circuit is such that energy stored in the inductor is confined to one output only and is not shared with the other outputs during the control and also, which allows controlling the output voltages with independent duty-cycles. As a result, the load voltage V_{01} (V_{02}) (V_{03}) is not influenced by the variation of load current i_{03} (i_{02}) (i_{01}). Hence the proposed configuration with this control approach avoids all the issues about cross-regulation problems even when the ground is involved during battery charging. More importantly, the configuration is simple and it can generate three independent outputs without any assumptions on inductor currents ($i_{L1} > i_{L2} > i_{L3}$ or $i_{L1} < i_{L2} < i_{L3}$ or $i_{L1} = i_{L2} = i_{L3}$) and/or operating duty cycle.

B. SEMICONDUCTOR STRESS ANALYSIS

Semiconductor stresses of the proposed configuration are presented Eq. (13)-(15) as [27].

1) VOLTAGE STRESSES

$$\begin{aligned} &V_{S_1} = V_{01}, \quad V_{D_1} = V_{01},\ V_{S_2} = \left(\frac{V_{02}+V_{DC}}{2}\right) \\ &V_{D_2} = (V_{02}+V_{DC}), \quad S_3 = V_{D_3} = V_{DC} \end{aligned} \tag{13}$$

2) CURRENT STRESSES

a: MODE 1

$$\begin{aligned} &i_{S_1} = i_{L_1}, \quad i_{D_1} = 0,\ i_{S_2} = i_{L_2}, \\ &i_{D_2} = 0, \quad i_{S_3} = i_{L_3},\ i_{D_3} = 0 \end{aligned} \tag{14}$$

b: MODE 2

$$\begin{aligned} &i_{S_1} = i_{D_1} = i_{L_1}, \quad i_{S_2} = i_{S_3} = 0, \\ &i_{D_2} = i_{L_1}, \quad i_{D_3} = i_{L_3} \end{aligned} \tag{15}$$

III. SMALL-SIGNAL MODELING

The transfer function of the proposed topology is derived from small signal analysis as [26]. The state-space equations (16)-(25) are as follows

$$[A]\,X(t) = Bx(t) + Cu(t) \tag{16}$$

$$y(t) = Dx(t) + Eu(t) \tag{17}$$

where state-space coefficients are A, B, C, D and E X(t) = state vector, U(t) = input vector, and y(t) = output vector

Where, State vector = $x(t)$, Input vector = $u(t)$ and Output vector = $y(t)$. (18)–(21), as shown at the bottom of the next page.

The output voltages $\hat{V}_{01}$ $\hat{V}_{02}$ and $\hat{V}_{03}$ are determined by $\hat{d}_1$ and $\hat{d}_2$, and $\hat{d}_3$

$$\hat{v}_{01}(s) = G_{vd1}\hat{d}_1(s),\ \hat{v}_{02}(s) = G_{vd2}\hat{d}_2(s),$$
$$\hat{v}_{03}(s) = G_{vd3}\hat{d}_3(s) \tag{22}$$

The proposed configuration control transfer function is given in Eq. (23-25) as follows

$$\frac{\hat{v}_{01}(s)}{\hat{d}_1(s)} = \frac{V_{DC}}{(1-D_1)^2}\left[\frac{1 - s\frac{L_1}{R_1(1-D_1)^2}}{1 + s\frac{L_1}{R_1(1-D_1)^2} + s^2\frac{L_1C_1}{(1-D_1)^2}}\right] \tag{23}$$

$$\frac{\hat{v}_{02}(s)}{\hat{d}_2(s)} = \frac{V_{DC}}{(1-D_2)^2}\left[\frac{1 - sD_2\frac{L_2}{R_2(1-D_2)^2}}{1 + s\frac{L_2}{R_2(1-D_2)^2} + s^2\frac{L_2C_2}{(1-D_2)^2}}\right] \tag{24}$$

$$\frac{\hat{v}_{03}(s)}{\hat{d}_3(s)} = V_{DC}\left[\frac{1}{1 + s\frac{L_3}{R_3} + s^2L_3C_3}\right] \tag{25}$$

The bode plot of the proposed configuration is illustrated in Figure 4 for verifying the stability. It is observed that the gain margin is 6.65 dB, 1.54 dB, and −1.55 dB, whereas the phase margin is 90° and 90° and 0.393° respectively for transfer functions of the proposed converter given in (23)-(25).

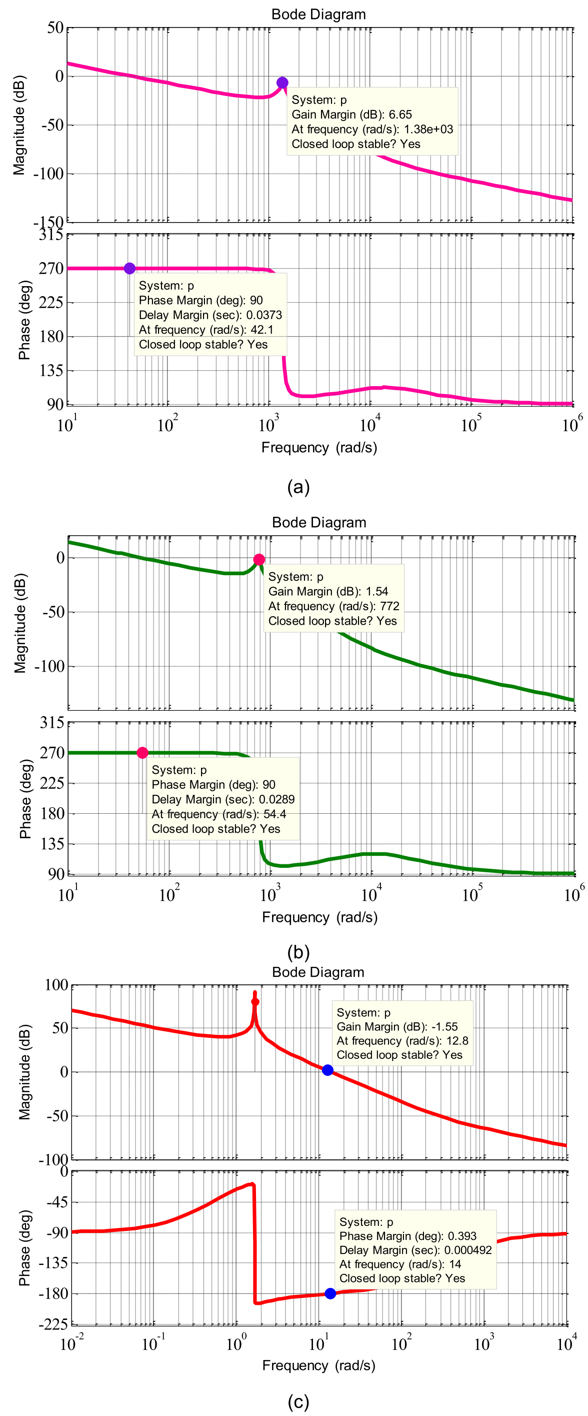

FIGURE 4. Bode plot of the proposed converter.

IV. CONTROLLER DESIGN, PARAMETER DESIGN, SMALL-SIGNAL MODELING, POWER LOSSES CALCULATIONS, AND COMPARATIVE ASSESSMENT

A. THE CONTROL METHOD OF THE PROPOSED CONVERTER

A suitable control scheme is essential for good voltage regulation. A control transfer function has been derived for each output by using small-signal modeling. It is cascaded with a controller, as illustrated in Figure 5, where the PI-controller is chosen as given (26) to reduce the undamped behavior of the system and improve the low-frequency performance, i.e., it reduces the steady-state error [18].

$$G_{c1}(s) = \left(\frac{K_Ps + K_I}{s}\right),\quad G_{c2}(s) = \left(\frac{K_Ps + K_I}{s}\right),$$
$$G_{c2}(s) = \left(\frac{K_Ps + K_I}{s}\right) \tag{26}$$

B. PARAMETERS DESIGN CONSIDERATIONS

The converter parameters design can be calculated using equations (27)-(29) as given in [27].

$$L_{1\,\min} = L_{2\,\min} = \frac{2}{27}\frac{R_{L\,\max}}{f_s},$$
$$L_{3\,\min} = \frac{R_{L\,\max}(1 - D_{\min})}{2f} \tag{27}$$

f_s = switching frequency, $D_{\min}$ = Minimum duty cycle

Calculation of filter capacitance value is

$$C_{1\min} = \frac{D_{\max} V_{01}}{V_{cpp} R_{L1\max} f_s}$$
$$C_{2\min} = \frac{D_{\max} V_{02}}{V_{cpp} R_{L2\max} f_s}, \quad C_{3\min} = \frac{D_{\max}}{2 r_c f_s} \tag{28}$$

where

$V_{01,02,03}$ = Output voltage, $D_{\max}$ = Maximum duty ratio, f_s = Switching frequency, $R_{L1,2\max}$ = Maximum load resistance, r_c = Maximum ESR of thefilter capacitor and V_{cpp} = Peak-to-peak value of the capacitor.

$$V_{cpp} = \frac{V_r}{2} \tag{29}$$

The ripple voltage (V_r) is 1% of V_0

C. POWER LOSSES CALCULATIONS

Power losses are essential for calculating efficiency as follows [28], [29], equations are presented in Eq. [30]–[35]

$$P_{loss\_IGBT} = P_{con} + P_{sw} \tag{30}$$

TABLE 2. Parameter specifications.

Parameter	Simulation	Experimental
Input voltage (V_{DC})	50 V	50 V
Output voltage ($V_{01}/V_{02}/V_{03}$)	100/50/25 V	100/50/25 V
Output currents ($I_{01}/I_{02}/I_{03}$)	2/2/2 A	2/2/2 A
Switching frequency (*f*)	50 kHz	50 kHz
Inductor ($L_1/L_2/L_3$)	0.6/0.9/1 mH	0.5/1/1 mH
Capacitor ($C_1/C_2/C_3$)	200/470/360 uF	220/470/470 uF

The IGBT conduction losses are

$$P_{con} = \frac{1}{T} \int_0^T (R_{on} i_F + V_{Fo}) i_F \, dt \tag{31}$$

R_{on} = Switch ON-state resistance, V_{Fo} = Threshold voltage, i_F = Forward current, and T = Switching period.

The switching losses are calculated as,

$$P_{sw} = (E_{OFF,j} + E_{ON,j}) \times f \tag{32}$$

where E_{ON} and E_{OFF} are and is the energy delivered in ON and OFF time of the power switches, respectively, and f is the switching frequency

$$P_L = r_L I_{Lrms}^2, \; I_{Lrms} = \frac{I_0}{(1-D)} \tag{33}$$

$$\frac{d}{dt}\begin{bmatrix} i_{L_1}(t) \\ i_{L_2}(t) \\ i_{L_3}(t) \\ v_{C_1}(t) \\ v_{C_2}(t) \\ v_{C_3}(t) \end{bmatrix} = B \begin{bmatrix} i_{L_1}(t) \\ i_{L_2}(t) \\ i_{L_3}(t) \\ v_{C_1}(t) \\ v_{C_2}(t) \\ v_{C_3}(t) \end{bmatrix} + CV_{DC} \tag{18}$$

$$B = \begin{bmatrix} 0 & 0 & 0 & -\left(\frac{1-D_1}{L_1}\right) & 0 & 0 \\ 0 & 0 & 0 & 0 & \left(\frac{1-D_2}{L_2}\right) & 0 \\ 0 & 0 & 0 & 0 & 0 & \left(\frac{1-D_3}{L_3}\right) \\ \left(\frac{1-D_1}{C_1}\right) & 0 & 0 & \frac{-1}{R_1 C_1} & 0 & 0 \\ 0 & \left(\frac{1-D_2}{C_2}\right) & 0 & 0 & \frac{-1}{R_2 C_2} & 0 \\ 0 & 0 & 0 & 0 & 0 & \frac{-1}{R_2 C_2} \end{bmatrix} \tag{19}$$

$$C = \begin{bmatrix} \frac{1}{L_1} \\ \frac{D_2}{L_2} \\ \frac{D_3}{L_3} \\ 0 \\ 0 \\ 0 \end{bmatrix} \tag{20}$$

$$D = \begin{bmatrix} 0 & 0 & 0 & 1 & 0 & 0 \\ 0 & 0 & 0 & 0 & 1 & 0 \\ 0 & 0 & 0 & 0 & 0 & 1 \end{bmatrix} \tag{21}$$

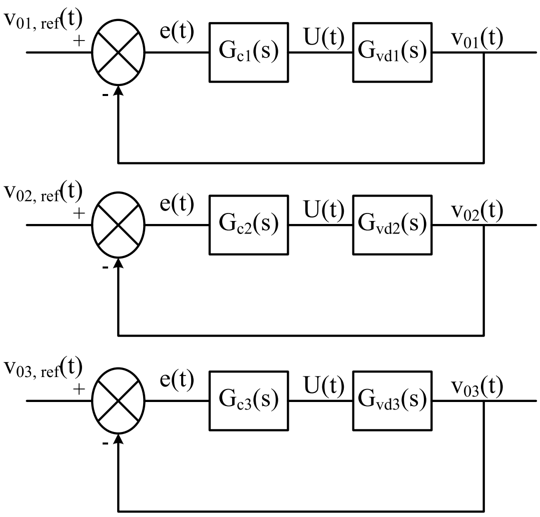

FIGURE 5. Closed-loop control system.

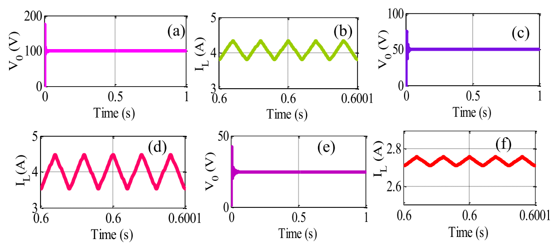

FIGURE 6. (a) V_{01}, (b) i_{L1}, (c) V_{03}, (d) i_{L2}, (e) V_0), (f) i_{L3}.

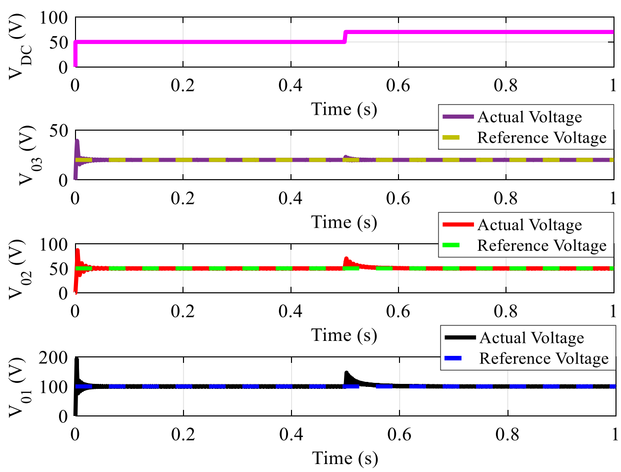

FIGURE 7. Performance of closed-loop control for a sudden variation in input voltage (V_{DC}) at 0.5 sec.

The power loss of the capacitor (P_C) is calculated as

$$P_C = r_C I_{Crms}^2, I_{Crms} = I_0\sqrt{\frac{D}{(1-D)}} \tag{34}$$

where I_{Lrms} is the RMS value of the inductor current and I_{Crms} RMMMS values of the capacitor current. $r_{C,}$ and r_L are the ESR of the capacitor and inductor, respectively.

The efficiency of the proposed converter is

$$\eta = \frac{P_{out}}{P_{out} + P_{sw} + P_{con} + P_L + P_C} \tag{35}$$

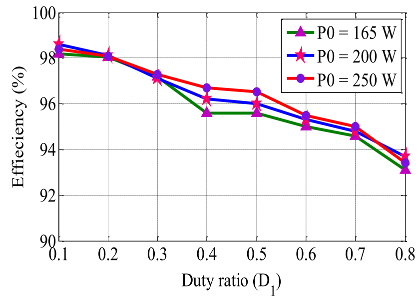

FIGURE 8. The efficiency of the proposed topology at different duty ratios.

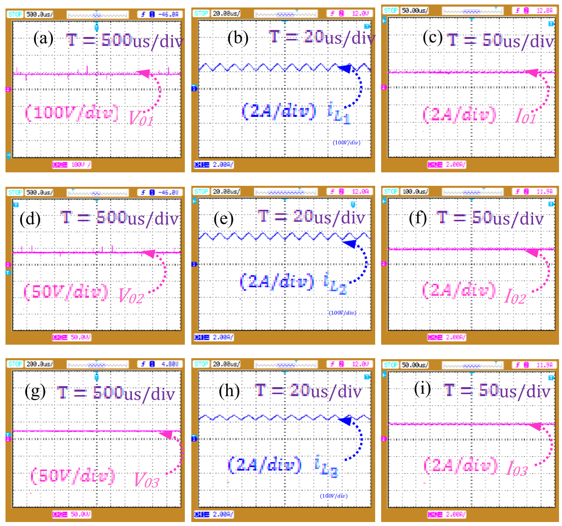

FIGURE 9. Experimental results: (a) V_{01}, (b) i_{L1}, (c) I_{01}, (d) V_{02}, (e) (i_{L2}), (f) (I_{02}), (g) V_{03}, (h) (i_{L3}) and (i) (I_{03}).

D. COMPARATIVE ASSESSMENT

The comparative assessment is presented in this section in terms of components, passive elements, and stresses on active switches for recently developed SIMO DC-DC converters in the literature.

1) THE NUMBER OF COMPONENTS

The comparative assessment based on the number of components has been done with recently reported single input multi output topologies as depicted in Table. 3. A single switch SIMO converter is presented in [15]; it reduces the control complexity of the system. Nevertheless, it may not be easy to regulate the outputs independently. A SIDO configuration is developed in [16] using a super-lift Luo-converter. It generates both step-up and step-down outputs. However, it has more components count. Reference [20] observed that the presented SIMO generates positive and negative output voltages. However, it increases the number of components that result in big size, high cost, and more power losses. The proposed converter in [18] has reduced part count and is suitable for EV auxiliary power supply applications. Nevertheless, it has such as $i_{L1} > i_{L2}$ for generating output voltages. In [21], a multi-output converter is developed with reduced components. Nevertheless, it may have high conduction losses due to more diodes. A new SIDO topology is

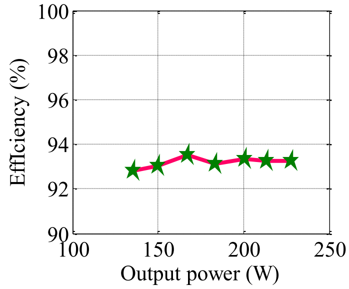

(a)

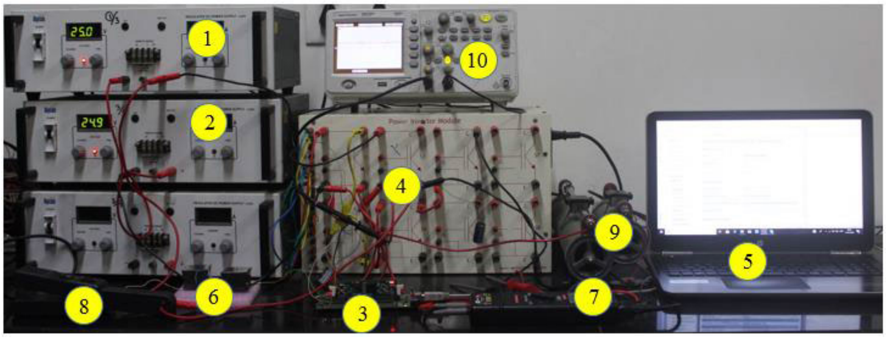

(b)

FIGURE 10. **(a) Efficiency of the proposed configuration, (b) Experimental setup developed in the laboratory: (1), (2) Voltage sources, (3) DSP 28335 Controller, (4) IGBT Module, (5) Host PC, (6), Inductor (L_1, L_2), (7) Differential probe, (8) Current probe, (9) Load (R), (10) DSO.**

presented in [22] has the advantages of low semiconductor stress and the size of the filter elements. However, it has more device count, which may affect the size of the power converter. A high-density multioutput converter is suggested in [23] for portable electronic applications, has more active switches, which may decrease the converter efficiency.

The comparison presented in Table 3 depicts that the proposed configuration is simple, and there are no assumptions on the inductor currents and operating duty ratio. It can generate three independent outputs and loads are isolated from each other during control and the cross-regulation problem is successfully eliminated.

2) VOLTAGE STRESS COMPARISON

The efficacy of the proposed configuration is also compared in terms of the voltage stress and is shown in Table 2. The maximum voltage stress of the proposed topology in [20] is the addition of input and output voltage. Similarly, topologies introduced in [18] and [22] have less voltage stress, i.e., half of the output voltage and supply voltage. The proposed configuration in [16] is the subtraction of output and supply voltage. The maximum voltage stress in the presented topology in [15] and proposed configuration is the output voltage. The suggested topology in [23] has low semiconductor stress. From Table 2, one can observe that the proposed topology has less semiconductor stress compared to suggested topologies in [16], [18], and [22]. The current stress on the switch is high in the presented topologies [18], and [20] is equal to the addition of inductor current. The proposed topology and converter proposed in [15], [16], [22], and [23] have less current stress, i.e., current flows through the one inductor (i_{L2}) only.

The proposed converter's comparative analysis has also been done in terms of control complexity and power density, as depicted in Table 4. The control complexity and power density are mainly dependent on the number of active switches and the total number of components in the power converter. It is observed that the topologies proposed in [19], [20], and [21] have a lesser number of active power switches as compared with [18], [22], [23], and the proposed topology. Hence they had low complexity in control. Similarly, the power density of any DC-DC converter mainly depends on the total number of components, especially active power switches, and they occupy more space. Consequently, the proposed power converter and topologies presented in [18], [20], and [22] have higher power densities.

Moreover, with the comparison of different aspects of power converter such as component count, semiconductor stresses, from Table. 2 suggests that each converter has its own merits and demerits. The proposed converter structure has low semiconductor stresses and avoids cross-regulation problems if the ground is involved during the charging of the input battery. The configuration is suitable for EVs' auxiliary power system applications.

V. RESULTS AND DISCUSSIONS

A. SIMULATION RESULTS

The model has been built in MATLAB environment to verify the proposed system with $V_{DC} = 50$ V, frequency is 50 kHz, and the duty ratio is 50%. The parameter details are

TABLE 3. Comparison between different SIMO topologies.

Ref.	G_{port}	$S_{V\_Stress}/S_{I\_Stress}$	$D_{V\_Stress}/D_{V\_Stress}$	N_S	N_D	N_L	N_C	$N_{component}$	N_{input}	N_{output}	Loads are isolated from each other during control
[15]	$V_{01}=\frac{D}{(1-D)}$, $V_{02}=\frac{1}{(1-D)}$ $D<1$	$V_{S\max}=V_{02}$ $i_{S\max}=i_{L_1}$	$V_{D\max}=V_g+V_{01}$ $i_{D\max}=i_{L_2}$	1	2	2	3	8	1	2	Yes
[16]	$V_{01}=\frac{V_{in}(2-D_2)}{(1-D_2)}$, $V_{02}=\frac{V_{in}(D_1-D_2)}{(1-D_2)}$ $D_2<D_1$	$V_{S\max}=V_{01}-V_{in}$ $I_{S\max}=I_{in}-I_{01}$	$V_{D\max}=V_{01}-V_{in}$ $I_{D\max}=I_{01}$	2	3	2	3	10	1	2	Yes
[18]	$V_{01}=D_1V_i, V_{02}=D_2V_i$ $D_1+D_2<1$	$V_{S\max}=V_i$ $V_{S_{0-2}}=V_i$ $i_{S\max}=i_{L_1}+i_{L_2}$		3	-	2	2	7	1	2	Yes
[20]	$V_{01}=\frac{V_{in}D}{(1-D)}$, $V_{02}=\frac{-V_{in}D}{(1-D)}$ $0<D<1$	$V_{S\max}=V_{in}+V_{02}$ $i_{S\max}=i_{L_1}+i_L$	$V_{D\max}=V_{in}+V_{02}$ $V_{D\max}=V_{01}-V_{02}$	2	3	2	3	10	1	2	Yes
[22]	$v_{01}=\frac{v_{in}}{(2-d_1-d_2)}$, $v_{02}=\frac{v_{in}(1-d_2)}{(2-d_1-d_2)}$ $0.5<d_1 \,\&\, d_2<1$	$V_{S\max}=\frac{V_{01}}{2}$ $i_{S\max}=i_{L_1}$		6	-	2	3	11	1	2	Yes
[23]	$V_{01}=\frac{2+D}{3}$, $V_{02}=\frac{1+D}{3}, V_{03}=\frac{D}{3}$ $0<D<1$	$V_{S\max}=V_{01}$ $i_{S\max}=i_{L_1}$		12	-	3	8	23	1	3	Yes
Proposed	$V_{01}=\frac{V_{DC}}{(1-D_1)}$ $V_{02}=\frac{D_2V_{DC}}{(1-D_2)}$ $V_{03}=D_3V_{DC}$ $0<D_1<1, 0<D_2<1,$ $0<D_3<1$	$V_{S\max}=V_{01}$ $i_{S\max}=i_{L_1}$	$V_{D\max}=V_{01}$ $i_{D\max}=i_{L_1}$	3	3	3	3	12	1	3	No

specified in Table. 2. The corresponding output voltages (V_{01}, V_{02}, and V_{03}) and inductor currents (i_{L1}, i_{L2}, and i_{L3}) are illustrated in Figure 6(a-f), respectively. The output voltages in Figures 6(a), 6(c) 6(e) are close to the theoretical results. The closed-loop control is implemented for the proposed configuration, and the dynamic performance of the overall system is validated for a sudden change in the input voltage. Figure 7. shows the simulation result of closed-loop control for a sudden change in the input voltage (V_{DC}) from 50V to 70 V at 0.5 sec. The PI control gains are chosen as $K_p = 0.1$ and $K_i = 15$ for Buck output, similarly $K_p = 0.005$ and $K_i = 0.5$ for Boost and Buck-Boost voltages.

TABLE 4. Comparison of complexity, power density, and efficiency.

Ref.	Complexity		Power density	
	Power switches	Complexity in controller design	Total number of components	Power density In each topology
20	S=2	Less	10	High
19	S=1	Less	24	Low
18	S=3	Less	7	High
21	S=2	Less	18	Low
22	S=4	Less	11	High
23	S=12	High	23	Low
Proposed	S=2	Less	12	High

The results show that the proposed configuration generates stiff independent output voltages and is not affected by the sudden change in supply. The efficiency of the proposed converter at different duty ratios and various power ratings is depicted in Figure 8.

B. EXPERIMENTAL VERIFICATION

The practical feasibility of the proposed configuration is tested on the laboratory prototype of the proposed converter. The parameter specifications of the designed prototype are given in Table 2. The control signals are generated using controller DSP 28335 for IGBT's (STGW30NC120HD). The test is conducted at $V_{DC} = 50$ V and $D_1 = D_2 = D_3 = 50\%$. The corresponding, Figure 9(a), 9(c), and 9(e) illustrates the output voltages (V_{01}, V_{02}, and V_{03}), inductor currents (i_{L1}, i_{L2}, and i_{L3}), and load currents (I_{01}, I_{02}, *and* I_{03}) are depicted in Figure 9(b), 9(d) and 9(f), respectively. Output voltages match the theoretical simulation results, i.e., Eq. (12), respectively. The converter efficiency at different output powers is illustrated in Figure 10(a), and the laboratory hardware experiment on the developed prototype circuit is shown in Figure 10(b).

VI. CONCLUSION

The structure of the SIMO converter is proposed in this paper. The operating principle and modes of operation have been explained in detail. The proposed configuration is simple and without assumptions on the charging of inductors and operating duty cycle. It can generate the buck, boost, and buck-boost output voltages with independent regulated voltages. Cross regulation problems do not exist in the proposed topology, so the sudden change in inductor and load currents does not affect the output voltages. Finally, simulation and experimental results validate the proposed converter operation and performance.

REFERENCES

[1] P. C. Heris, Z. Saadatizadeh, and E. Babaei, "A new two input-single output high voltage gain converter with ripple-free input currents and reduced voltage on semiconductors," *IEEE Trans. Power Electron.*, vol. 34, no. 8, pp. 7693–7702, Aug. 2019, doi: 10.1109/TPEL.2018.2880493.

[2] A. Farakhor, M. Abapour, and M. Sabahi, "Design, analysis, and implementation of a multiport DC–DC converter for renewable energy applications," *IET Power Electron.*, vol. 12, no. 3, pp. 465–475, Mar. 2019.

[3] S. K. Mishra, K. K. Nayak, M. S. Rana, and V. Dharmarajan, "Switched-boost action based multiport converter," *IEEE Trans. Ind. Appl.*, vol. 55, no. 1, pp. 964–975, Jan./Feb. 2019.

[4] X. Lu, K. L. V. Iyer, C. Lai, K. Mukherjee, and N. C. Kar, "Design and testing of a multi-port sustainable DC fast-charging system for electric vehicles," *Electr. Power Compon. Syst.*, vol. 44, no. 14, pp. 1576–1587, Aug. 2016.

[5] E. Babaei and O. Abbasi, "A new topology for bidirectional multi-input multi-output buck direct current–direct current converter," *Int. Trans. Electr. Energ. Syst.*, vol. 27, no. 2, pp. 1–15, Feb. 2017.

[6] Z. Rehman, I. Al-Bahadly, and S. Mukhopadhyay, "Multiinput DC–DC converters in renewable energy applications—An overview," *Renew. Sustain. Energy Rev.*, vol. 41, pp. 521–539, Jan. 2015.

[7] G. Chen, Y. Liu, X. Qing, and F. Wang, "Synthesis of integrated multi-port DC–DC converters with reduced switches," *IEEE Trans. Ind. Electron.*, vol. 67, no. 6, pp. 4536–4546, Jun. 2019.

[8] P. Patra, A. Patra, and N. Misra, "A single-inductor multiple-output switcher with simultaneous buck, boost, and inverted outputs," *IEEE Trans. Power Electron.*, vol. 27, no. 4, pp. 1936–1951, Apr. 2012.

[9] M. Abbasi, A. Afifi, and M. R. A. Pahlavani, "Comments on 'a single-inductor multiple-output switcher with simultaneous buck, boost, and inverted outputs,'" *IEEE Trans. Power Electron.*, vol. 34, no. 2, pp. 1980–1984, Feb. 2019.

[10] Y.-C. Hsu, J.-Y. Lin, C.-H. Wang, and S.-W. Chou, "An SIMO step-down converter with coupled inductor," in *Proc. Int. Symp. VLSI Design, Autom. Test (VLSI-DAT)*, Hsinchu, Taiwan, Aug. 2020, pp. 1–4, doi: 10.1109/VLSI-DAT49148.2020.9196435.

[11] G. Nayak and S. Nath, "Comparing performances of SIDO buck converters," in *Proc. IEEE Int. Conf. Power Electron., Drives Energy Syst. (PEDES)*, Chennai, India, Dec. 2018, pp. 1–6.

[12] Y. Zheng, J. Guo, and K. N. Leung, "A single-inductor multiple-output buck/boost DC–DC converter with duty-cycle and control-current predictor," *IEEE Trans. Power Electron.*, vol. 35, no. 11, pp. 12022–12039, Nov. 2020.

[13] X. Zhang, B. Wang, X. Tan, H. B. Gooi, H. H.-C. Iu, and T. Fernando, "Deadbeat control for single-inductor multiple-output DC–DC converter with effectively reduced cross regulation," *IEEE J. Emerg. Sel. Topics Power Electron.*, vol. 8, no. 4, pp. 3372–3381, Dec. 2020.

[14] J. D. Dasika, B. Bahrani, M. Saeedifard, A. Karimi, and A. Rufer, "Multivariable control of single-inductor dual-output buck converters," *IEEE Trans. Power Electron.*, vol. 29, no. 4, pp. 2061–2070, Apr. 2014.

[15] E. Durán, S. P. Litrán, and M. B. Ferrera, "Configurations of DC–DC converters of one input and multiple outputs without transformer," *IET Power Electron.*, vol. 13, no. 12, pp. 2658–2670, Sep. 2020.

[16] B. Faridpak, M. Farrokhifar, M. Nasiri, A. Alahyari, and N. Sadoogi, "Developing a super-lift Luo-converter with integration of buck converters for electric vehicle applications," *CSEE J. Power Energy Syst.*, vol. 7, no. 4, pp. 811–820, Jul. 2021, doi: 10.17775/CSEEJPES.2020.01880.

[17] O. Ray, A. Josyula, S. Mishra, and A. Joshi, "Integrated dual-output converter," *IEEE Trans. Ind. Electron.*, vol. 62, no. 1, pp. 371–382, Jan. 2015.

[18] G. Chen, Y. Deng, J. Dong, Y. Hu, L. Jiang, and X. He, "Integrated multiple-output synchronous buck converter for electric vehicle power supply," *IEEE Trans. Veh. Technol.*, vol. 66, no. 7, pp. 5752–5761, Jul. 2017.

[19] M. S. B. Ranjana, N. S. Reddy, and R. K. P. Kumar, "A novel sepic based dual output DC-DC converter for solar applications," in *Proc. Power Energy Syst., Towards Sustain. Energy*, Mar. 2014, pp. 1–5.

[20] J. Marjani, A. Imani, E. Afjei, and A. Hekmati, "A new dual output DC-DC converter with enhancing output voltage level," in *Proc. 24th Iranian Conf. Electr. Eng. (ICEE)*, May 2016, pp. 573–577.

[21] Z. Saadatizadeh, P. C. Heris, E. Babaei, and M. Sabahi, "A new nonisolated single-input three-output high voltage gain converter with low voltage stresses on switches and diodes," *IEEE Trans. Ind. Electron.*, vol. 66, no. 6, pp. 4308–4318, Jun. 2019.

[22] A. Ganjavi, H. Ghoreishy, and A. A. Ahmad, "A novel single-input dual-output three-level DC–DC converter," *IEEE Trans. Ind. Electron.*, vol. 65, no. 10, pp. 8101–8111, Oct. 2018.

[23] S. M. Ahsanuzzaman, A. Prodic, and D. A. Johns, "An integrated high-density power management solution for portable applications based on a multioutput switched-capacitor circuit," *IEEE Trans. Power Electron.*, vol. 31, no. 6, pp. 4305–4323, Jun. 2016.

[24] M. Y. Hassani, M. Maalandish, and S. H. Hosseini, "A new single-input multioutput interleaved high step-up DC–DC converter for sustainable energy applications," *IEEE Trans. Power Electron.*, vol. 36, no. 2, pp. 1544–1552, Feb. 2021.

[25] E. D. Aranda, S. P. Litrán, and M. B. F. Prieto, "An interleaved single-input multiple-output DC-DC converter combination," *CSEE J. Power Energy Syst.*, vol. 8, no. 1, pp. 132–142, Jan. 2022, doi: 10.17775/CSEEJPES.2020.00300.

[26] V. Ramanarayanan, *Course Material on Switched Mode Power Conversion*. Bangalore, India: IISc., Jan. 2008.

[27] M. K. Kazimierczuk, *Pulse-Width Modulated DC-DC Power Converters*, 1st ed. Hoboken, NJ, USA: Wiley, 2008.

[28] R. S. Alishah, D. Nazarpour, S. H. Hosseini, and M. Sabahi, "Reduction of power electronic elements in multilevel converters using a new cascade structure," *IEEE Trans. Ind. Electron.*, vol. 62, no. 1, pp. 256–269, Jan. 2015.

[29] N. Sandeep and U. R. Yaragatti, "Operation and control of a nine-level modified ANPC inverter topology with reduced part count for grid-connected applications," *IEEE Trans. Ind. Electron.*, vol. 65, no. 6, pp. 4810–4818, Jun. 2018.

MUDADLA DHANANJAYA was born in Andhra Pradesh, India. He received the B.Tech. degree in electrical and electronics engineering and the M.Tech. degree in power electronics and electric drives from JNTUK, Kakinada, India, in 2011 and 2013, respectively, and the Ph.D. degree in power electronics from the National Institute of Technology, Raipur, in 2020. In 2019, he joined as an Assistant Professor with the Anil Neerukonda Institute of Technology and Sciences, Visakhapatnam, Andhra Pradesh. His current research interests include high gain dc–dc converters, multiport dc–dc converters, and multilevel inverters.

DEVENDRA PONURU (Senior Member, IEEE) was born in Andhra Pradesh, India. He received the B.Tech. degree in electrical and electronics engineering from Nagarjuna University, Guntur, in 2000, the Master of Engineering (M.E.) degree from the University College of Engineering, Anna University, Guindy, Chennai, in 2002, and the Ph.D. degree in power electronics and drives from JNTU, Kakinada, in 2016. His current research interests include high gain dc–dc converters, multiport dc–dc converters, and control of electric machines.

THANIKANTI SUDHAKAR BABU (Senior Member, IEEE) received the B.Tech. degree from Jawaharlal Nehru Technological University, Anantapur, India, in 2009, the M.Tech. degree in power electronics and industrial drives from Anna University, Chennai, India, in 2011, and the Ph.D. degree from VIT University, Vellore, India, in 2017.

He is currently working as an Associate Professor with the Department of Electrical Engineering, Chaitanya Bharathi Institute of Technology (CBIT), Hyderabad, India. He had completed his Postdoctoral Researcher Fellowship from the Institute of Power Engineering, Universiti Tenaga Nasional (UNITEN), Malaysia. Before to that, he was worked as an Assistant Professor at the School of Electrical Engineering, VIT University. He has published more than 100 research articles in various renowned international journals. His research interests include the design and implementation of solar PV systems, renewable energy resources, power management for hybrid energy systems, storage systems, fuel cell technologies, electric vehicles, and smart grids. He has been acting as an Associate Editor of *IET RPG*, IEEE ACCESS, *ITEES* (Wiley), and *Frontiers in Energy Research*; a Section Editor of *Energies* (MDPI) and *Sustainability* (MDPI); and a reviewer for various reputed journals.

BELQASEM ALJAFARI received the master's degree in electrical engineering from Northern Illinois University, USA, in 2016, and the Ph.D. degree in electrical engineering from the University of South Florida, USA, in 2019. He is currently working as an Assistant Professor with the Electrical Engineering Department, Najran University, Saudi Arabia. His research interests include power and renewable energy, electrochemical energy storage, solar cells, and nano materials.

HASSAN HAES ALHELOU (Senior Member, IEEE) is currently a Faculty Member with Tisheen University, Lattakia, Syria, and Monash University, Australia. He was with University College Dubline (UCD), Ireland, as a Senior Researcher. He serves as a Consultant at Sultan Qaboos Universit, Oman. He has published more than 30 research papers in the high-quality peer-reviewed journals and international conferences. He has also performed more than 160 reviews for high prestigious journals, including IEEE TRANSACTIONS ON INDUSTRIAL INFORMATICS, IEEE TRANSACTIONS ON INDUSTRIAL ELECTRONICS, *Energy Conversion and Management*, *Applied Energy*, and *International Journal of Electrical Power and Energy Systems*. He has participated in more than 15 industrial projects. His major research interests include power systems, power system dynamics, power system operation, and control, dynamic state estimation, frequency control, smart grids, micro-grids, demand response, load shedding, and power system protection. He is included in the 2018 and 2019 Publons List of the Top 1% Best Reviewer and Researchers in the field of engineering. He was a recipient of the Outstanding Reviewer Award from *Energy Conversion and Management* journal, in 2016; *ISA Transactions* journal, in 2018; *Applied Energy* journal, in 2019; and many other awards. He was a recipient of the Best Young Researcher in the Arab Student Forum Creative among 61 researchers from 16 countries at Alexandria University, Egypt, in 2011.